KSME

Springer

Journal of Mechanical Science and Technology 37 (11) 2023

Original Article
DOI 10.1007/s12206-023-1029-x

Keywords:
· Compressible flow
· Projectile launch
· Pressure wave
· Shock wave

Correspondence to:
Hyoungsoon Lee
leeh@cau.ac.kr;
Jaiyoung Ryu
jryu@korea.ac.kr

[#] These authors equally contributed to this manuscript.

Citation:
Sung, W., Kim, J., Jang, K. S., Le, T. T. G., Kim, J., Kim, D. H., Lee, H., Ryu, J. (2023). Parametric study of a projectile launched by a compressed air cannon. Journal of Mechanical Science and Technology 37 (11) (2023) 5913~5933.
http://doi.org/10.1007/s12206-023-1029-x

Received April 13th, 2023
Revised July 20th, 2023
Accepted July 24th, 2023

† Recommended by Editor Han Seo Ko

Parametric study of a projectile launched by a compressed air cannon

Woojin Sung[1,#], Jihoon Kim[2,#], Kyeong sik Jang[1], Thi Thanh Giang Le[3], Jeonglae Kim[4], Dong Hyeon Kim[5], Hyoungsoon Lee[1,3] and Jaiyoung Ryu[1,2]

[1]Department of Mechanical Engineering, Chung-Ang University, Seoul 06974, Korea, [2]School of Mechanical Engineering, Korea University, Seoul 02841, Korea, [3]Department of Intelligent Energy and Industry, Chung-Ang University, Seoul 06974, Korea, [4]School for Engineering of Matter, Transport and Energy, Arizona State University, Tempe, AZ 85287, USA, [5]Hyper Tube Express (HTX) Research Team, Korea Railroad Research Institute, Gyeonggi-do 16105, Korea

Abstract The principle of the compressed air cannon is that compressed air in the reservoir expands rapidly to propel the projectile. Previous studies assume that the tube pressure in front of the projectile is constant because the tube pressure was too low compared to the compressed air pressure in the reservoir. However, when the projectile actually travels in the tube, a compression wave is generated in front of the projectile. In this study, the theoretical prediction for the velocity of the projectile was performed using the tube pressure in front of the projectile affected by the compression wave as a variable. The results show that the maximum velocity decreases compared to previous studies. This difference from the constant tube pressure assumption cases becomes larger as the maximum velocity of the projectile increases. The theoretical prediction considering the compression wave shows a more realistic deceleration than when the tube pressure is constant.

1. Introduction

A compressed air cannon is typically used to build launched systems such as guns, and cannon weapons by physically analyzing the flow around a projectile fired within a long closed tube. The compressed air cannon comprises a reservoir, projectile, and closed tube.

The operating principle of the compressed air cannon is that the compressed air in the reservoir expands rapidly, transmitting force to the projectile, which is fired and moved within the closed tube. Because the performance of the compressed air cannon is mostly expressed in terms of the velocity of the projectile, theoretical developments for predicting the velocity of the compressed air cannon have been made in many studies. Rohrbach et al. applied the conservation of momentum, work-kinetic energy theorem, and Newtonian mechanics when designing the compressed air cannon to predict the velocity of the projectile [1]. Further, Mungan predicted the velocity of the projectile by applying the first law of thermodynamics to the compressed air expansion process under a reversible and adiabatic process [2].

Denny applied the expansion process of the compressed air as an isothermal process and analyzed the velocity of the projectile for travel distance and constant friction force between the projectile and the wall [3]. In addition, Ayars et al. predicted the distance and velocity of the projectile using the characteristic length [4]. These studies developed the theory by focusing only on the pressure of the compressed air expanding behind the projectile. In other words, these studies neglected the tube pressure in front of the projectile because is usually atmospheric pressure, which is very low compared to the initial pressure of the compressed air in the reservoir.

However, in actual operation, when the projectile travels within the closed tube, the compression wave is generated in front of the projectile [5-11]. This compression wave increases the tube pressure in front of the projectile and disturbs its movement, thereby reducing its velocity [12]. Auvity and Bellenoue studied the propagation of the pressure wave in a tube, and they found that a compression wave is generated when a body moves at subsonic speed [13]. The compression wave induces a high-pressure region owing to the air compressibility effect compression wave induces a high-pressure region owing to the air compressibility effect [14]. Although the high-pressure region is considerably smaller compared to the pressure of the compressed air behind the projectile, it is expected that this will reduce the velocity of the projectile.

Therefore, the main objective of this study is to analyze the behavior of the projectile through theory development considering the effect of the compression wave generated in front of the projectile. The theoretical model for predicting the behavior of the projectile assumes the tube pressure in front of the projectile as a variable to consider the effect of the compression wave. In the process, a shock-fixed coordinate is applied to the compressed air cannon to consider the compression wave [15]. So far, previous studies have not mentioned which process is more suitable for the expansion process of the compressed air behind the projectile when analyzing the compressed air cannon [1]. Therefore, in this study, both processes were considered to compare the effect of the compression wave acting on the projectile for the expansion process of the compressed air.

The next section develops the theory by assuming the tube pressure affected by the compression wave as a variable. The results section shows the velocity and travel distance of the projectile for the change in the cross-sectional area and mass of the projectile and change in the initial pressure of the compressed air for each expansion process of the compressed air through the developed theoretical model.

2. Theoretical development

Fig. 1 shows each model according to the time and tube pressure in front of the projectile for the compressed air cannon used in this study for theory development.

Fig. 1(a) shows the initial process of the compressed air cannon before the projectile is propelled at time t = 0 s.

Further, Fig. 1(b) shows the model from the previous study, where the projectile has traveled by a distance x during time t without considering the compression wave. Fig. 1(c) shows that the projectile travels by a distance x during time t in a model that considers the compression wave in this study. Because the compression wave is considered, the tube pressure in front of

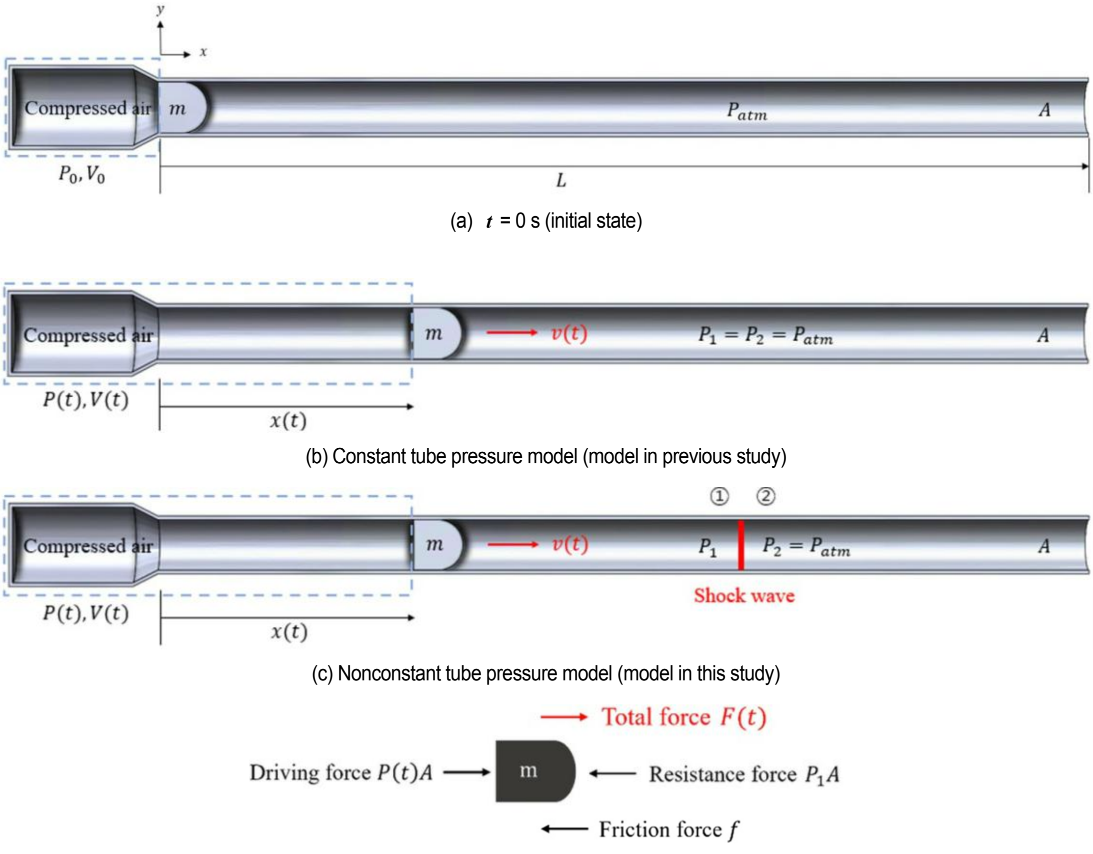

(a) t = 0 s (initial state)

(b) Constant tube pressure model (model in previous study)

(c) Nonconstant tube pressure model (model in this study)

(d) Schematic of the force acting on the projectile

Fig. 1. Illustration of a compressed air cannon according to time and tube pressure in front of the projectile: (a) t = 0 s is the initial state of the compressed air cannon; in (b) and (c), the blue line dash box represents the rapidly expanding compressed air distribution; in (c), ① and ② indicate local points in the rear and front of the shock wave, respectively, and the pressure at that location is indicated by subscripts 1 and 2. P_{atm} means the value of 1 atm; in (d), arrows show the direction of the force acting on the projectile.

the projectile is divided into rear and front regions of the compression wave. Therefore, the tube pressure P_2 in front of the compression wave, which is not yet affected by the compression wave, is assumed to be a constant value, and the tube pressure P_1 at the rear of the compression wave that has already been affected by the compression wave is assumed as a variable.

The reservoir contains compressed air with an initial volume V_0 and an initial pressure P_0. In this study, the air inside the entire system, including the compressed air in the reservoir, is assumed to be an ideal gas. During time t, the projectile with mass m travels as distance x in the closed tube of total length L owing to the rapidly expanding compressed air from the reservoir. $P(t)$ and $V(t)$ are the pressure and volume, respectively, of the compressed air behind the projectile changing during time t. The friction force f that occurs between the projectile and the tube exists because the cross-sectional area A of the projectile is assumed to be equal to the cross-sectional area of the tube.

In addition, as the cross-sectional areas are the same, there is no effect on leakage of the compressed air behind the projectile. Furthermore, the projectile is assumed to have no rotational motion while traveling in the closed tube [3, 4]. Therefore, it is assumed that there is no Magnus force, a force perpendicular to the rotation of the projectile [16]. In Fig. 1(c), the projectile travels in the tube by driving force given by the rapid expansion of the compressed air behind the projectile. As mentioned earlier in the introduction, this study both considers the isothermal process and isentropic process.

First, when the expansion process of the compressed air is applied as the isothermal process, it is assumed to be a quasi-equilibrium process [1]. As in quasi-equilibrium, when the expansion process of the compressed air proceeds slowly, sufficient time is given for heat exchange until the compressed air reaches the same temperature as the surrounding environment. Therefore, it is possible to apply the expansion process of the compressed air as the isothermal process.

Conversely, when the expansion process of the compressed air is applied as the isentropic process, it is assumed that the process is reversible and very fast. Assuming that the expansion process is so fast that there is not enough time to transfer heat to the surroundings, it can be said that there is no heat transfer to the outside like an adiabatic process [2, 17, 18]. Therefore, the expansion process of the compressed air can also be applied as the isentropic process.

The theory developed in this study applies the isothermal process and the isentropic process to the expansion process of the compressed air, respectively, and compares the results. The above assumptions applied to the expansion process of the compressed air do not directly affect the flow between the projectile and the compression wave.

Next, in Fig. 1(d), the equation for the force acting on the projectile of the compressed air cannon is as follows:

$$F(t) = P(t)A - P_1A - f = ma(t) . \quad (1)$$

Where $P(t)$ is the pressure of the compressed air expanding behind the projectile during time t, P_1 is the tube pressure in front of the projectile (rear of the compression wave). Further, F represents the total force acting on the projectile, m represents the mas of the projectile, and a represents the acceleration of the projectile. In Eq. (1), the force acting on the projectile can be divided into driving force $P(t)A$, resistance force P_1A, and friction force f [8]. The pressure $P(t)$ is expressed differently depending on whether the expansion process of the compressed air behind the projectile is the isothermal process or the isentropic process.

The friction force f generated between the projectile and the tube wall and affects the behavior of the projectile together with the tube pressure in front of the projectile. The flow behind the compression wave from the front of the projectile is assumed to be isentropic and inviscid, except across the compression wave. This isentropic process is assumed to be independent of the friction force developed between the projectile and the tube wall. In addition, the flow ignores boundary layer formation and flow separation from the tube walls. The flow is assumed to be a quasi-one-dimensional flow to capture main properties such as the compression wave [15, 19, 20]. The parameter for the thickness of the shock wave was not analyzed because there was no heat conductivity effect [21].

2.1 Expansion process of the compressed air

In this study, assuming the tube pressure in front of the projectile as a variable to consider the compression wave, we developed a theory to predict the behavior of the projectile in the isothermal and isentropic processes of the expansion process of the compressed air, respectively. Moreover, as mentioned above, the compressed air in the reservoir behind the projectile was assumed to be an ideal gas. First, when the expansion process of the compressed air is applied as an isothermal process, the volume of the compress air is inversely proportional to its pressure according to the ideal gas equation $PV = C$. Therefore, the pressure $P(t)$ and volume $V(t)$ of the expanding compressed air behind the projectile with respect to time t can be expressed as follows:

$$P_0V_0 = P(t)V(t) . \quad (2)$$

From Fig. 1, $V(t)$ can be expressed as follows:

$$V(t) = V_0 + Ax(t) . \quad (3)$$

By using Eqs. (2) and (3), $P(t)$ can be expressed as the following equation:

$$P(t) = P_0\left(\frac{V_0}{V_0 + Ax(t)}\right) . \quad (4)$$

$P(t)$ is expressed as an equation according to the travel distance x of the projectile as per Eq. (3). Therefore, the force equation of the projectile in the isothermal process is derived by substituting Eq. (4) into Eq. (1).

$$F = ma(t) = P_0\left(\frac{V_0}{V_0 + Ax(t)}\right)A - P_1 A - f \,. \tag{5}$$

Eq. (5) for the force acting on the projectile comprises the initial pressure and initial volume of the compressed air, cross-sectional area A of the projectile, friction force f between the projectile and the tube wall, travel distance x of the projectile, and the tube pressure P_1 in front of the projectile.

Eq. (5) cannot be used to directly calculate the behavior of the projectile because the variables are x, P_1, and f. Therefore, Eq. (5) can be solved using the normal shock wave relation by assuming that tube pressure P_1 is a variable considering the compression wave. This is explained in the next section. The friction force f actually varies from case to case. However, the friction force is usually analyzed by ignoring it or assuming it to be constant [3, 9]. In this study, we simplified the model by adopting the calculation of the friction force by Denny to easily analyze the behavior of the projectile for the friction force [3]. Denny expressed the friction force as the initial pressure of the compressed air and the cross-sectional area of the barrel. Since the cross-sectional area is constant, the friction force is expressed as a ratio of 0-1 from the initial pressure of the compressed air behind the projectile. In addition, we assume that the friction force is constant regardless of the velocity of the projectile. Sasoh et al. quantitatively evaluated the friction force both theoretically and experimentally and concluded that the friction force can become comparable with the driving force made by the propellant gas when the fit between the projectile and the tube is tight [22]. Our study simplified the friction force without defining a kinetic friction model like above study. However, our study assumes that the cross-sectional area of the projectile is equal to the cross-sectional area of the tube, so the fit can be assumed to be tight.

Therefore, we assume that the frictional force acting on the projectile, which is the dimensionless frictional force 1 (maximum friction), is equal to the initial driving force $P_0 A$ acting on the projectile, which means that the projectile is at rest.

Next, when the expansion process of the compressed air is applied as the isentropic process, the pressure and volume of the compressed air at time t can be expressed by the ideal gas equation as follows:

$$\frac{P(t)}{P_0} = \left(\frac{V_0}{V(t)}\right)^{\gamma} . \tag{6}$$

The initial state of the projectile (before the projectile is propelled) x (0) = 0, P (0) = P_0, V (0) = V_0 is shown in Fig. 1(a). In Eq. (6), γ represents the specific heat ratio of air. Using Eq. (3) as the volume term in Eq. (6), the pressure of the expanding air during time t is expressed as follows:

$$P(t) = P_0\left(\frac{V_0}{V_0 + Ax(t)}\right)^{\gamma} . \tag{7}$$

Substituting Eq. (7) into Eq. (1), which is the equation of force acting on the projectile, we get

$$F = ma(t) = P_0\left(\frac{V_0}{V_0 + Ax(t)}\right)^{\gamma} A - P_1 A - f \,. \tag{8}$$

Eq. (8) is an expression for the isentropic process and is the same as the isothermal process that is derived from Eq. (5) except for the specific heat ratio. Similarly, the behavior of the projectile cannot be directly determined as the variables are x, P_1 and f. Therefore, as in the isothermal process, Eq. (8) can be solved by expressing the friction force f in the dimensionless range of 0-1 and assuming the tube pressure P_1 as a variable.

2.2 Compression wave in front of the projectile

In this section, the theoretical development is described only when the expansion process of the compressed air is the isentropic process. This is because the theoretical development of the isothermal process and the isentropic process for the expansion process of the compressed air are almost same (only the specific heat ratio term is added). We apply Newton's law of motion and the normal shock wave relation to obtain the tube pressure P_1 in front of the projectile, which is assumed as a variable to consider the compression wave.

First, initial state values of the projectile need to be defined to predict the behavior of the projectile. Therefore, when the projectile is in the initial state t_0 before being launched, Newtons' second law of motion is applied to obtain the travel distance x_0, velocity v_0, acceleration a_0 of the projectile. The acceleration a_0 of the projectile at time t_0 is expressed by substituting x_0 into the Eq. (8) of the force acting on the projectile as follows:

$$a_0 = \frac{A}{m}\left[P_0\left(\frac{V_0}{V_0 + Ax_0}\right)^{\gamma} - P_1 - \frac{f}{A}\right]. \tag{9}$$

The acceleration of the projectile is expressed with respect to time t using $adt = dv$ as follows:

$$a(t) = \frac{dv}{dt} = \frac{A}{m}\left[P_0\left(\frac{V_0}{V_0 + Ax(t)}\right)^{\gamma} - P_1 - \frac{f}{A}\right]. \tag{10}$$

Therefore, integrating from t_0 to t, the velocity v of the projectile over time is expressed as:

$$\int_{v_0}^{v} dv = \int_{t_0}^{t} \frac{A}{m}\left[P_0\left(\frac{V_0}{V_0 + Ax_0}\right)^{\gamma} - P_1 - \frac{f}{A}\right]dt \ . \tag{11}$$

In Eq. (11), the initial pressure P_0 of the compressed air, cross-sectional area A of the projectile, mass m of the projectile, and time t are the values set in this study. In addition, the travel distance x_0 of the projectile before it is launched is 0 m, so the velocity v_0 of the projectile is 0 m/s. Therefore, In Eq. (11), the velocity v of the projectile integrating from t_0 to t is an equation with only the variable P_1. Furthermore, in this study, the dimensionless friction is given as an initial condition to eliminate the friction force f, which is a variable. That is, the friction force f is expressed in the form of dimensionless 0-1 using the initial pressure of the compressed air behind the projectile and the cross-sectional area of the projectile.

Finally, P_1 can be obtained by applying the normal shock wave relation. The schematic of the normal shock wave generated in the compressed air cannon system is shown in the figure below.

The velocity $v_1^s = v_1 - v_s$ can be seen from the shock-fixed coordinates in Fig. 2(c). Thus, the equation for v_1 is expressed as follows:

$$v_1 = v_s + v_1^s \ . \tag{12}$$

In this study, the flow properties across the compression wave have been quantified by applying the normal shock wave relations. Except for the flow across the compression wave, the flow fields are assumed to be isentropic. Therefore, Eq. (12) is expressed in terms of the Mach number by dividing it by $\sqrt{\gamma RT_1}$, which is derived from the isentropic equation [23].

$$M_1 = \frac{v_s}{\sqrt{\gamma RT_1}} - M_1^s \ . \tag{13}$$

Where M_1^s is the transformed representation from $v_1^s / \sqrt{\gamma RT_1}$, and v_1^s is a negative value because the velocity of the compression wave is faster than the projectile by applying the normal shock wave relation. Therefore, the sign in front of M_1^s is negative. To convert the first term on the right side of Eq. (13) into M^S, $v_s / \sqrt{\gamma RT_1}$ is expressed as follows:

$$\frac{v_s}{\sqrt{\gamma RT_1}} \times \frac{\sqrt{\gamma RT_2}}{\sqrt{\gamma RT_2}} \ . \tag{14}$$

$v_s / \sqrt{\gamma RT_2}$ becomes M_s, leaving the term $\sqrt{\gamma RT_2} / \sqrt{\gamma RT_1}$, and Eq. (13) is converted as follows:

$$M_1 = M_s \times \frac{\sqrt{\gamma RT_2}}{\sqrt{\gamma RT_1}} - M_1^s \ . \tag{15}$$

The Mach number M_s of the compression wave is the same as the Mach number M_2^s of the flow ② in Fig. 2(c) according to the concept of the normal shock wave relation. Therefore, Eq. (15) can be expressed as follows:

$$M_1 = M_2^s \times \frac{\sqrt{\gamma RT_2}}{\sqrt{\gamma RT_1}} - M_1^s \ . \tag{16}$$

When the second term on the right side in Eq. (16) is converted into a normal shock wave relation, it becomes as follows:

$$\sqrt{\frac{\gamma RT_2}{\gamma RT_1}} = \sqrt{\frac{(\gamma+1)^2 (M_2^s)^2}{\left[2\gamma (M_2^s)^2 - (\gamma-1)\right] \times \left[(\gamma-1)(M_2^s)^2 + 2\right]}} \tag{17}$$

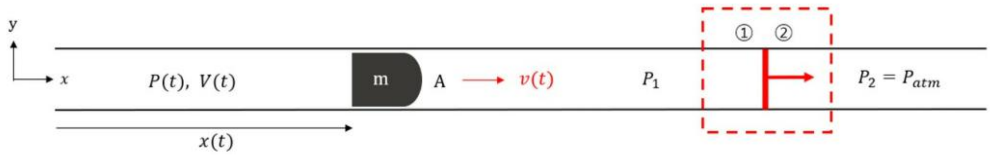

(a) Schematic of compressed air cannon tube

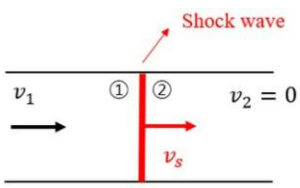

(b) Absolute coordinates

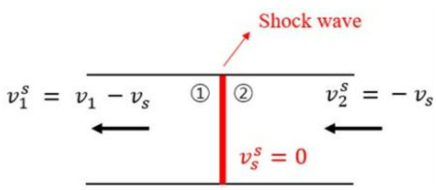

(c) Shock-fixed coordinates

Fig. 2. Schematic of the shock wave and flow velocity in different coordinate systems. The superscript s indicates the velocity in shock-fixed coordinates, and the velocity in absolute coordinates is shown without the superscript. ① and ② indicate local points behind and in front of the shock wave, respectively; the velocity at those locations is indicated by subscripts 1 and 2, and the subscript s indicates the propagation velocity of the shock wave.

Furthermore, the Mach number M_1^s of flow ① in Eq. (16) can be expressed as follows by using the normal shock relation:

$$M_1^s = \sqrt{\frac{(\gamma-1)M_2^s+2}{2\gamma\left(M_2^s\right)^2-(\gamma-1)}} . \tag{18}$$

Finally, by substituting Eqs. (17) and (18) into Eq. (16), it is expressed as follows:

$$\begin{aligned} M_1 = M_2^s \times \sqrt{\frac{(\gamma+1)^2\left(M_2^s\right)^2}{\left[2\gamma\left(M_2^s\right)^2-(\gamma-1)\right]\times\left[(\gamma-1)\left(M_2^s\right)^2+2\right]}} \\ -\sqrt{\frac{(\gamma-1)M_2^s+2}{2\gamma\left(M_2^s\right)^2-(\gamma-1)}} . \end{aligned} \tag{19}$$

In the study of the Hyperloop system, Jang et al. mentioned that, under isentropic and inviscid assumptions, the flow quantities do not vary from the behind of the shock wave to the nose of the pod (the vehicle in the Hyperloop system) [15]. It is also explained that for high-speed projectiles, the most significant acceleration occurs near the breech, keeping the velocity of the projectile relatively constant over the most of the latter portion of its in-bore trajectory [8, 24]. In our study, the projectile moves at high speed due to the high pressure behind the projectile. Also, the flow between the projectile and the compression wave is assumed to be isentropic and quasi-steady inviscid flow. Therefore, we assume that the Mach number of the flow ① is equal to the Mach number of the projectile. The Mach number M_1 of the flow ① can be expressed as the velocity v_1 of the projectile using the speed of sound relation:

$$M_1 = \frac{v_1}{\sqrt{\gamma R T_1}} . \tag{20}$$

Substituting Eq. (20) into Eq. (19) to expressed it as an equation for v_1,

$$v_1 = \sqrt{\gamma R T_1} \times \left[\begin{aligned} M_2^s \times \sqrt{\frac{(\gamma+1)^2\left(M_2^s\right)^2}{\left[2\gamma\left(M_2^s\right)^2-(\gamma-1)\right]\times\left[(\gamma-1)\left(M_2^s\right)^2+2\right]}} \\ -\sqrt{\frac{(\gamma-1)M_2^s+2}{2\gamma\left(M_2^s\right)^2-(\gamma-1)}} \end{aligned} \right] . \tag{21}$$

Eq. (21) for the velocity of the projectile is expressed as a function of M_2^s. Therefore, the velocity of the projectile can be obtained by assuming that the velocity v of the projectile over time in Eq. (11) derived previously and the velocity v_1 of the projectile in Eq. (21) to which the normal shock wave relation is applied are the same. First, Eq. (11) for the velocity of the projectile over time is expressed as a function only of M_2^s by applying the normal shock wave relation.

In Eq. (11) for the acceleration of the projectile according to time t, P_1 is expressed according to the normal shock wave relation as follows:

$$\begin{aligned} & a(t) = \frac{dv}{dt} = \frac{A}{m}\left[P_0\left(\frac{V_0}{V_0+Ax(t)}\right)^{\gamma} - P_1 - \frac{f}{A}\right], \\ & \frac{P_1}{P_2} = \frac{2\gamma\left(M_2^S\right)^2-(\gamma-1)}{\gamma+1} . \end{aligned} \tag{22}$$

By substituting Eq. (22) into Eq. (11), from time t_0 to t it is expressed as follows:

$$\int_{v_0}^{v} dv = \int_{t_0}^{t} \frac{A}{m}\left[P_0\left(\frac{V_0}{V_0+Ax_0}\right)^{\gamma} - P_2\left(\frac{2\gamma\left(M_2^S\right)^2-(\gamma-1)}{\gamma+1}\right) - \frac{f}{A}\right] dt . \tag{23}$$

Therefore, because the v_1 in Eq. (21) and the v in Eq. (23) have the same variable M_2^S, Eqs. (21) and (23) are combined to obtain M_2^S. Then the velocity v of the projectile integrated from t_0 to t can be obtained using M_2^S. Moreover, the travel distance x over the same time interval can be obtained using the velocity v, and similarly the acceleration a of the projectile can be obtained using x. Our theoretical model could predict the velocity, distance, and acceleration of the projectile from time t_0 to t. The theoretical model was repeated to obtain continuous values over time for the compressed air cannon. The results (described in Sec. 3) were obtained at intervals of 0.00001 s for a total projectile travel distance time of 0.03 s.

3. Results and discussion

The parameters used in the analysis were applied as the same values presented in the reference study [3]. The reference study was analyzed assuming the maximum pressure of 200 atm for the air gun charging the gas reservoir under the pressure range of 70-200 atm. In the study, the equation for the force acting on the pellet neglects the effect of the tube pressure in front of the pellet. This is because the tube pressure is atmospheric pressure, which is very small compared to the initial pressure of the compressed air. However, our study considers tube pressure. Therefore, in order to apply the same force to the pressure acting on the projectile as in the reference study, our study set the initial pressure of the compressed air to 201 atm and the initial pressure of the tube to 1 atm.

In other words, the initial pressure and initial volume of the compressed air in the reservoir were set to P_0 = 201 atm and V_0 = 1.6×10^{-5} m^3. Next, the cross-sectional area A of the projectile was 2.5×10^{-5} m^2, which was the specification of the

Table 1. Comparison of the characteristics of the main parameters of the compressed air cannon required for each analysis. For example, ID CP201 represents the constant tube pressure model and initial pressure of the compressed air (201 atm).

Tube pressure type	Initial pressure of the reservoir (atm)	ID
Constant	201	CP201
Nonconstant	11	NP011
Nonconstant	51	NP051
Nonconstant	101	NP101
Nonconstant	201	NP201

0.22 caliber gun. The mass m of the projectile was 1.0×10^{-3} kg, which was the specification of the 0.22 pellet. The above parameter values vary in each case and are given in Table 1. Table 1 lists the IDs classified according to the tube pressure type and the initial pressure of the compressed air.

The tube pressure type in Table 1 is expressed as constant when the tube pressure is assumed to be constant without considering the compression wave, and nonconstant when the tube pressure is assumed as a variable considering the compression wave.

There is only one constant type, while the nonconstant type is divided into 4-four types according to the initial pressure of the compressed air. Sec. 3.1 compares the tube pressure type to be nonconstant and the tube pressure type to be constant. The result is expressed as the maximum velocity v_{max} of the projectile, acceleration of the projectile, maximum velocity occurrence point of the projectile, and maximum travel distance x_{max} of the projectile. Sec. 3.2 shows the result of analyzing the case only where the tube pressure type is nonconstant. Sec. 3.2.1 describes the pressure of the compression wave, Mach number of the compression wave, velocity of the projectile, acceleration of the projectile, and travel distance of the projectile over time. Further, Sec. 3.2.2 analyzes the effect of change in the cross-sectional area and mass of the projectile on the velocity and travel distance of the projectile. Finally, Sec. 3.2.3 evaluates the effect of the initial pressure change of the compressed air in the reservoir on the velocity and travel distance of the projectile. Our study results are for the assumption that the compression wave does not reach the end of the tube in all cases.

The dimensionless friction f_d displayed in the plot of each section represents the range of 0-1. As mentioned above, f_d is the initial condition expressed dimensionless of range 0-1 by dividing the friction force by the product of the initial pressure of the compressed air and the cross-sectional area of the projectile. The friction force refers to that generated between the projectile and the tube wall, as mentioned above, and has no direct effect on the compression wave. The dimensionless friction is expressed as follows:

$$f_d = \frac{f}{P_0 A}. \tag{24}$$

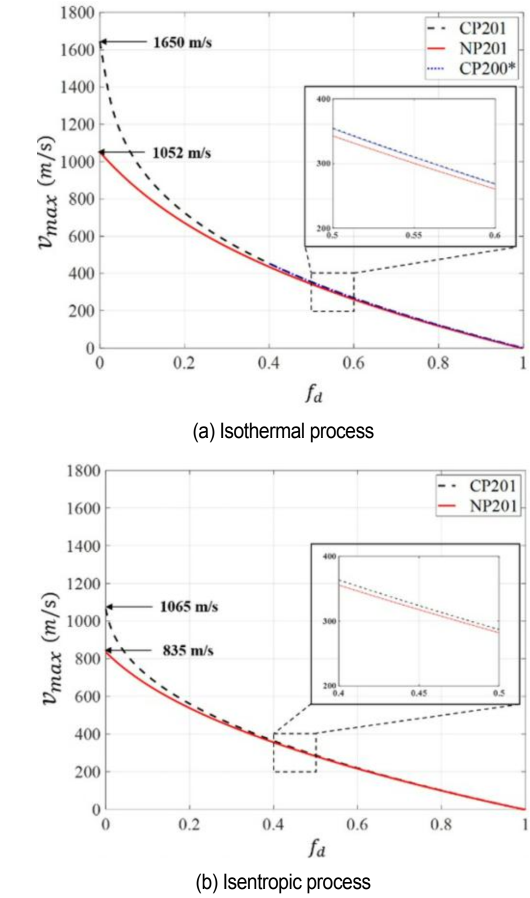

Fig. 3. Comparison of the maximum velocity v_{max} of the projectile versus the dimensionless friction f_d for the constant and the nonconstant tube pressure in (a) isothermal process; (b) isentropic process. f_d denotes the dimensionless friction, and the specifications for each ID are given in Table 1.

3.1 Comparison of nonconstant and constant tube pressure models

This section compares the case where the tube pressure is assumed as a variable considering the compression wave and the case where the tube pressure is assumed as a constant without considering the compression wave. The tube pressure in front of the projectile, which does not consider the compression wave, was fixed at 1 atm.

The comparison was made under the same conditions except that the tube pressure type was different. In addition, the results of references were used to validate the results of CP of this study [3]. Here, CP represents constant tube pressure model, and NP represents nonconstant tube pressure model. The results of references are indicated with superscripts *.

Fig. 3 shows the maximum velocity v_{max} of the projectile corresponding to each point within the range 0-1 of the dimensionless friction. In Fig. 3, (a) isothermal process and (b) isentropic process represent the expansion process of the compressed air behind the projectile, and the enlarged part in the figure shows the trend of v_{max}. In the case of NP201, the

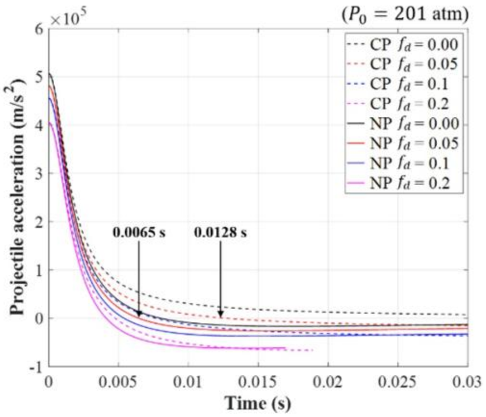

(a) Isothermal process

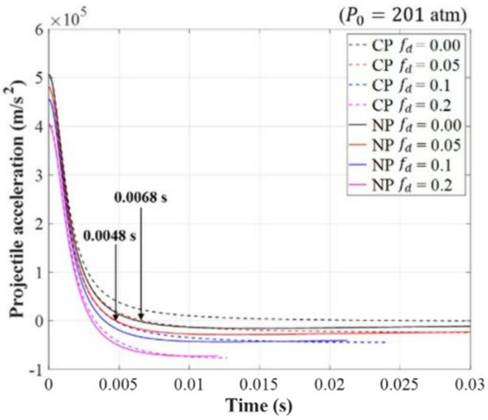

(b) Isentropic process

Fig. 4. Acceleration of the projectile for the constant and nonconstant tube pressure in the (a) isothermal process; (b) isentropic process in the dimensionless friction range of 0-0.2. For example, CP- f_d = 0.2 represents the acceleration of the projectile when the dimensionless friction is 0.2 in the constant tube pressure model.

maximum velocity of the projectile for each dimensionless friction was obtained using the theory derived in Sec. 2. In the case of CP201, the initial pressure of the compressed air was assumed to be 201 atm, and the tube pressure in front of the projectile was assumed to be 1 atm. By assuming that the tube pressure was a constant, the normal shock wave relation was not used.

Therefore, CP201 obtained the maximum velocity of the projectile at each dimensionless friction over time in the same way as NP201 except for the normal shock wave relation. For CP200*, the result of the reference study ignores the tube pressure in front of the projectile and assumes the initial pressure of the compressed air to be 200 atm [3]. Therefore, in all cases, the pressure difference between the front and rear of the projectile was 200 atm.

The results show the maximum velocity of the projectile for each dimensionless friction within an arbitrarily set projectile travel time of 0.03 s. Accordingly, this study confirmed that the maximum velocity NP201 decreased compared to CP201 in both the cases where the compressed air was assumed to be the isothermal process and isentropic process.

The enlarged part reveals, that the maximum velocity of NP201 was lower than the maximum velocity of CP201 in the entire section of the dimensionless friction. In the isothermal process, the difference in maximum velocity between the CP201 and NP201 was 36 % and 6 % at dimensionless friction of 0 and 0.9, respectively.

As dimensionless friction decreases, the maximum velocity decrease rate of the projectile increases. CP201 showed almost the same results as CP200* with dimensionless friction ranging from 0.4 to 1, as seen in the enlarged part of Fig. 3(a). Therefore, the results of CP201 and NP201 were confirmed as the difference from assuming that the tube pressure in front of the projectile was a variable considering the compression wave.

The maximum velocity of the projectile was higher overall in the isothermal process than in the isentropic process. When the pressure of the ideal gas decreases and the volume of the ideal gas expands, the isentropic process does not exchange heat with the outside. However, the isothermal process can do more work because it receives heat from the outside to maintain a constant temperature. Therefore, the maximum velocity of the projectile is higher in the isothermal process.

Fig. 4 shows the acceleration of the projectile for the dimensionless friction in the range 0-0.2, which can explain the tendency of the difference in the maximum velocity of the projectile when the dimensionless friction is low.

In Figs. 4(a) and (b), when f_d is 0, NP can be seen that the maximum velocity appears faster than CP by 0.02 s or more owing to the effect of the compression wave. As the friction force acting on the projectile decreases, the velocity of the projectile increases. As the velocity of the projectile increases, the magnitude of the compression wave increases, but the compression wave eventually affects the behavior of the projectile. Thus, the compression wave in front of the projectile reduces the acceleration of the projectile.

When the dimensionless friction is 0.05 in the isothermal process, the maximum velocity occurrence time of NP is 0.0065 s and CP is 0.0128 s. Further, when the dimensionless friction is 0.05 in the isentropic process, the maximum velocity occurrence time of NP is 0.0048 s and CP is 0.0068 s. The maximum velocity of the projectile occurs at the point where the acceleration of the projectile decreases and becomes negative, and this point appears faster in the isentropic process than in the isothermal process.

Fig. 5 shows the maximum velocity occurrence point of the projectile corresponding to each point within the range 0-1 of the dimensionless friction f_d . CP200* is the result of the reference study for validating CP201, as shown in Fig. 3. The enlarged part of Fig. 5(a) reveals that CP201 and CP200* show almost identical results. As with the result of v_{max} , it was confirmed that the result of the NP201 considering the compression wave lower than that of CP201 without considering the compression wave. Therefore, the maximum velocity of NP201 is reached faster than CP201, after which the velocity of the projectile decreases. The difference in the effect of these

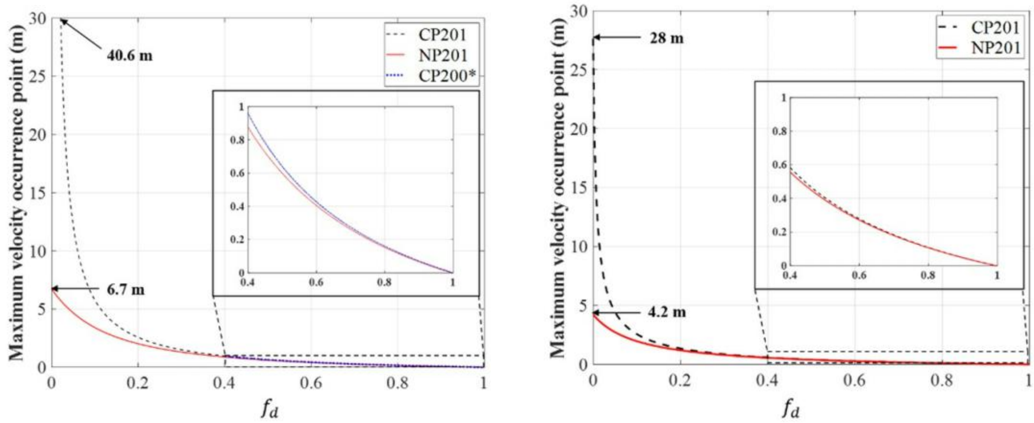

(a) Isothermal process (b) Isentropic process

Fig. 5. Comparison of the maximum velocity occurrence point versus the dimensionless friction f_d for the constant and nonconstant tube pressure in (a) isothermal process; (b) isentropic process. f_d represents the dimensionless friction, and the specifications for each ID are given in Table 1.

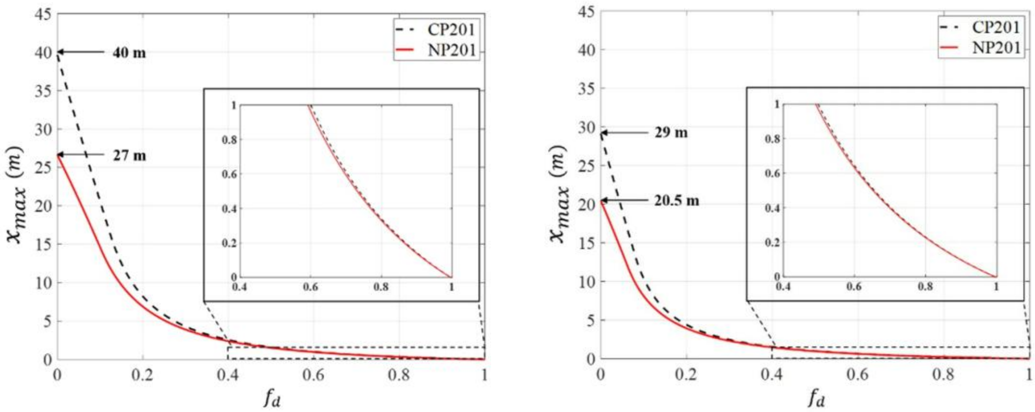

(a) Isothermal process (b) Isentropic process

Fig. 6. Comparison of the maximum travel distance x_{max} versus the dimensionless friction f_d for the constant and nonconstant tube pressure in the (a) isothermal process; (b) isentropic process. f_d denotes the dimensionless friction and the specifications for each ID are given in Table 1.

is that the com pression wave increases as the friction force decreases. In particular, when the dimensionless friction is 0, the isothermal process decreases by 83.5 % and the isentropic process decreases by 85 %, indicating that the effect of the compression wave is very significant. In the case of CP201, when the dimensionless friction is 0, the resistance force acting on the traveling projectile is due to only 1 atm of the tube pressure in front of the projectile, which shows that there is significant difference from the NP201.

Fig. 6 shows the maximum travel distance of the projectile corresponding to each point within the range 0-1 of the dimensionless friction f_d. The maximum travel distance of the projectile shows the same tendency as the maximum velocity of the projectile and the maximum velocity occurrence point. The result obtained by NP201 was overall lower than CP201. In addition, the result was lower in the isentropic process than in the isothermal process.

In the isentropic process, CP201 showed 27.5 % lower results and NP201 showed 24 % lower results than those in the isothermal process. In the case of CP, when the maximum velocity occurrence point in Fig. 5 and the maximum travel distance in Fig. 6 were compared both the isothermal and isentropic processes, almost similar results were obtained.

Therefore, in the case of CP, the maximum velocity of the projectile appeared when the projectile almost reached the end of the tube. Conversely, in the case of NP, the maximum velocity of the projectile reached faster than that of CP, and then the velocity decreased.

3.2 Analysis of the nonconstant tube pressure model

In this section, the results of analyzing only the nonconstant tube pressure type are shown to analyze the effect of the compression wave generated in the front of the projectile on the compressed air cannon. The pressure P_2 in front of the compressed wave was fixed at 1 atm. When the dimensionless friction is 1.0, the projectile is in a stationary state, so the range

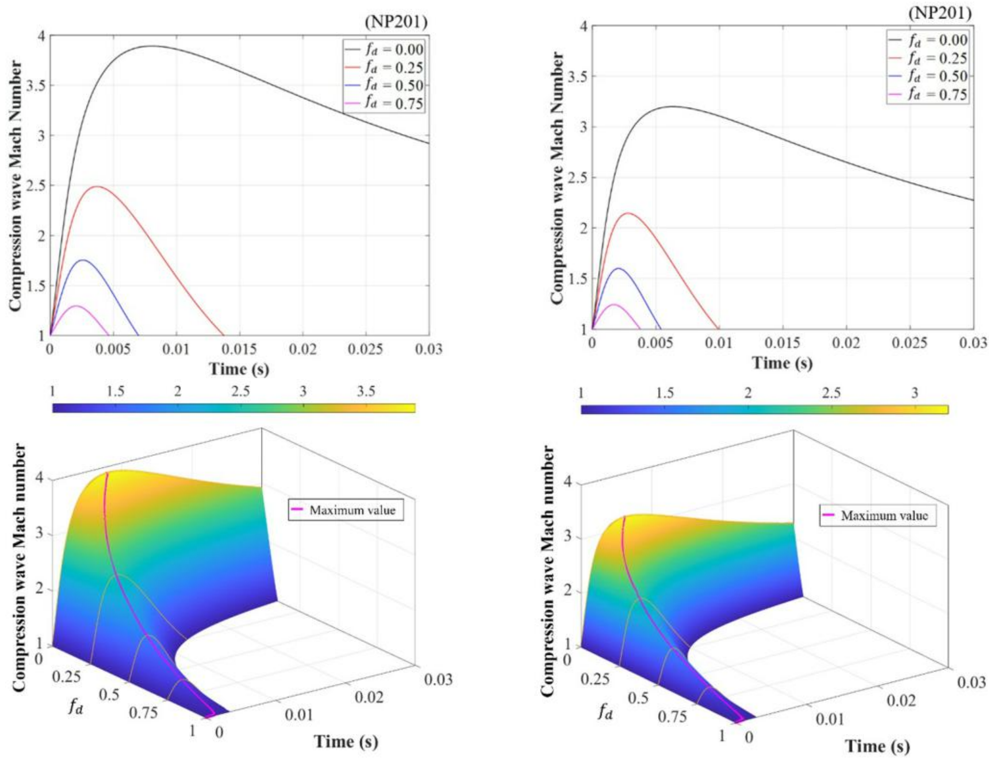

(a) Isothermal process

(b) Isentropic process

Fig. 7. Compression wave Mach number versus time for the nonconstant tube pressure in each process: (a) isothermal process; (b) isentropic process both using the case of NP201, where f_d is the dimensionless friction. The compression wave Mach number is expressed as a three-dimensional plot, and the maximum value is expressed as a line plot.

0-0.75 excluding 1.0 was analyzed by dividing by 0.25. Jiang assumed that the frictional force is 25 %, 50 %, and 75 % of the drag force, and performed three cases and obtained the result. Our study represents the effect of compression waves for 0.25, 0.5, and 0.75 of dimensionless friction including zero dimensionless friction.

As mentioned above, the travel time of the projectile is 0.03 s in total, showing the results of performing iterations at 0.00001 s intervals. Sec. 3.2.1 shows the results of analyzing the Mach number of the compression wave, pressure of the compression wave, velocity of the projectile, and travel distance of the projectile in the isothermal and isentropic processes to analyze the effect of the compression wave on the projectile.

In Sec. 3.2.2, the effect of the compression wave on the projectile when the mass and cross-sectional area of the projectile increase is analyzed with the velocity and travel distance of the projectile. In Sec. 3.2.3, the effect of the compression wave on the projectile when the initial pressure of the compressed air behind the projectile increases is analyzed with the velocity and the travel distance of the projectile.

3.2.1 Analysis of compression wave mach number, compression wave magnitude, projectile velocity, projectile acceleration, and projectile travel distance

In this study, the compression wave Mach number, compression wave pressure, velocity of the projectile, acceleration of the projectile, and travel distance of the projectile were analyzed by applying the theoretical model derived in Sec. 2.2. The cross-sectional area A of the projectile, mass m of the projectile, and initial pressure P_0 and volume V_0 of the compressed air were used the same as in Sec. 3.1.

The compression wave Mach number is results of M_2^s from Sec. 2.2 and was obtained over time by iterating our theoretical model by applying the normal shock wave relation. The compression wave pressure is P_1, which is the pressure behind the compression wave or in front of the projectile, and represents the results obtained by Eq. (22). The velocity, acceleration, and travel distance of the projectile are given using the Mach number M_2^s of the compression wave.

In Fig. 7, the compression wave Mach number increases rapidly as the projectile accelerates after launch and then decreases after the maximum value. The Mach number of the compression wave is 1 at 0 s. At 0 s, the velocity of the projectile is 0 m/s, but it has an initial acceleration owing to the propulsion of the expanding air behind the projectile. This initial acceleration of the projectile creates a disturbance in the flow in front of the projectile.

Thus, the disturbance of the flow in front of the projectile creates the shock wave with Mach number 1. When the initial compression wave Mach number is 1, the tube pressure P_1 behind of the compression wave has the same value (1 atm) as the tube pressure P_2 in front of the compression wave according to Eq. (22). Then, as the projectile travels, the magnitude behind and in front of the compression wave becomes the same again and the Mach number becomes 1, so the projectile stops. In addition, as the dimensionless friction increases, the velocity of the projectile decreases significantly, so the Mach number of the compression wave also decreases significantly.

The Mach number of (a) the isentropic process is lower than that of (b) the isothermal process as a whole. When the dimensionless friction is 0, the maximum Mach number of compression wave in the isentropic process is 0.693 (18 %) lower than that of the isothermal process, and the average of the maximum Mach number difference is 0.216 in the range of 0-1 of f_d . The travel time of the projectile was confirmed to be longer in the isothermal process than in the isentropic process.

Fig. 8 shows the compression wave magnitude (= pressure P_1 behind the compression wave) according to the travel time of the projectile. The compression wave magnitude shows a decrease to 1 atm after a maximum value at a dimensionless friction higher than 0.063 for a travel time of 0.03 s. Actually, the friction force is different depending on the case, but in this study, the friction force is expressed as the ratio of the initial pressure of the compressed air and the cross-sectional area of the projectile. However, because the cross-sectional area of the projectile is constant, the friction force changes according to the initial pressure of the compressed air. Therefore, as the compressed air pressure behind the projectile is much larger than the compression wave magnitude, the effect of the friction force is more dominant than the effect of the compression wave, so this result is shown. For both processes, the travel time for the maximum peak of compression wave magnitude is equal to that for the maximum compression wave Mach number. Overall, the compression wave magnitude shows the same increasing and decreasing trend as the compression wave Mach number.

Moreover, in the isentropic process, the compression wave magnitude decreases faster to 1 atm than in the isothermal process over the entire dimensionless friction ranges. For both isothermal and isentropic processes, the maximum value of compression wave magnitude is approximately 20 times lower than the initial pressure of the compressed air of 201 atm for all dimensionless friction.

Fig. 9 shows the velocity of the projectile over time by performing iteration and is the results including the constant tube pressure type to analyze the effect of the compression wave. In Fig. 9(a), except for the case where the dimensionless friction of the constant tube pressure type is 0, the velocity of the projectile increases rapidly after launch and then decreases after the maximum velocity.

The maximum velocity of the projectile occurs at the traveling time when the compression wave Mach number attains the

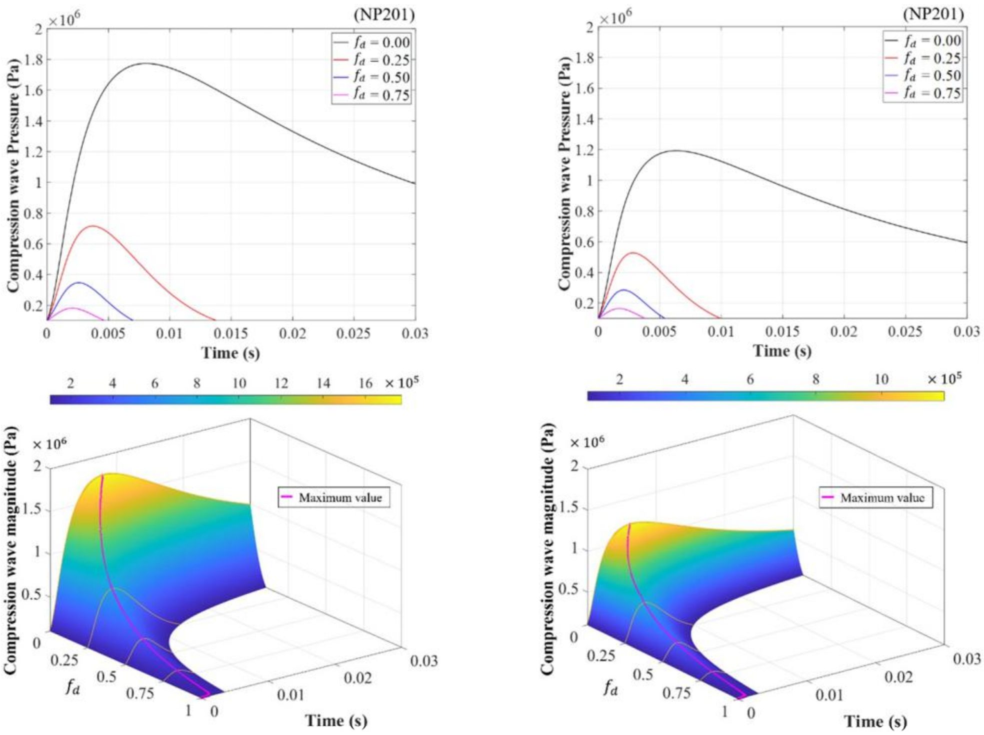

(a) Isothermal process (b) Isentropic process

Fig. 8. Compression wave magnitude versus time for Nonconstant tube pressure in each process: (a) Isothermal process; (b) isentropic process both using the case of NP201, where f_d is the dimensionless friction. The compression wave magnitude is expressed as a three-dimensional plot, and the maximum value is expressed as a line plot.

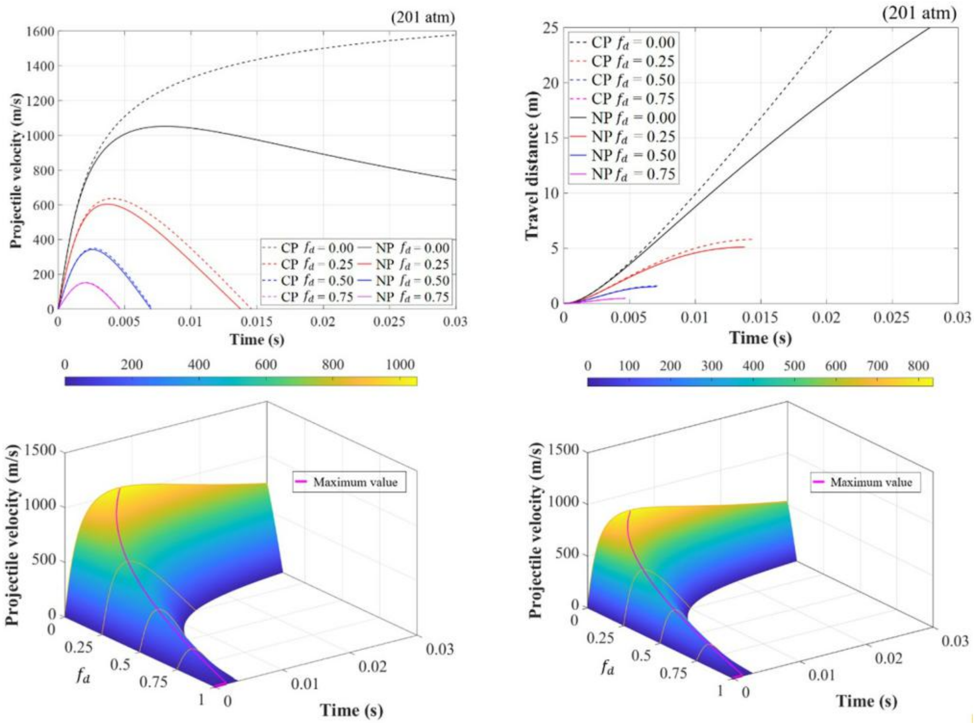

(a) Isothermal process (b) Isentropic process

Fig. 9. Velocity of the projectile over time in the isothermal and isentropic processes. CP is the constant tube pressure type, NP is the nonconstant tube pressure type, and f_d is the dimensionless friction. The velocity of the projectile expressed as a three-dimensional plot shows the results of NP201, and the maximum value is expressed as a line plot.

maximum value. In particular, the compression wave magnitude, compression wave Mach number, and velocity of the projectile reach their maximum values at the same travel time.

This is because, as assumed in Sec. 2.2, the Mach number of flow ① in Fig. 2 is assumed to be the same as that of the projectile. Thus, the velocity of the projectile is a result of the Mach number of flow ①.

The velocity of the projectile decreases to 0 m/s in the same travel time as when the compression wave Mach number decreases to 1. In the isentropic process rather than in the isothermal process, the pressure of the compressed air propelling the projectile is lower owing to the specific heat ratio. Therefore, the velocity of the projectile is lower because the force propelling the projectile is smaller in the isentropic process.

When the dimensionless friction is 0, the velocity of the projectile continues to increase with travel time of the projectile in both processes. However, in the case of NP, it represents that the velocity of the projectile decreases according to the travel time of the projectile in both processes owing to the effect of the compression wave. In particular, it can be seen that the lower the dimensionless friction, the greater the decrease in the velocity of the projectile owing to the effect of the compression wave.

Fig. 10 shows the acceleration of the projectile from 0 to 0.75 in intervals of 0.25 excluding the dimensionless friction of 1. The Mach number of the compression wave, pressure of the compression wave, and velocity of the projectile attain their maximum values simultaneously. This indicates that the acceleration of the projectile has these maximum values at the time it becomes negative. When the dimensionless friction is about 0.53 (friction force is 270 N) in the isothermal process and when the dimensionless friction is about 0.52 (friction force is 263 N) in the isentropic process, the minimum acceleration of the projectile increases.

Fig. 10 shows that when the dimensionless friction is 0.75, the minimum acceleration is higher than the minimum acceleration when it is 0.5. In other words, as the dimensionless friction force increases, the amount of reduction decreases as the initial acceleration decreases, so this is phenomenon is shown.

In addition, the initial acceleration of the projectile has the same value for both the isothermal and isentropic processes. Thereafter, as the projectile travels, the acceleration decreases, thereby decreasing in the isentropic process. As the acceleration decreases, the velocity of the projectile reduces, and the travel time decreases as the projectile travels a shorter distance.

Fig. 11 shows the travel distance of the projectile from 0 to 0.75 in intervals of 0.25, excluding the dimensionless friction 1. The result of iterating over time intervals. In Fig. 11(a), the projectile of the NP travels up to 0.45 m with the dimensionless friction of 0.75. Here, in the case of CP with the dimensionless friction of 0.75, the travel distance and travel time of the projectile are almost the same as those of NP with a difference of

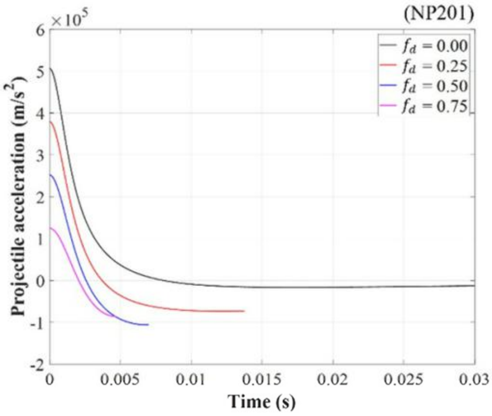

(a) Isothermal process

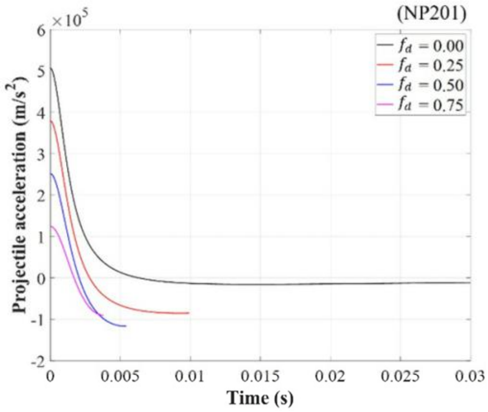

(b) Isentropic process

Fig. 10. Acceleration of the projectile over time in each process for nonconstant tube pressure: (a) Isothermal; (b) isentropic processes both using the case of NP201, where f_d is the dimensionless friction.

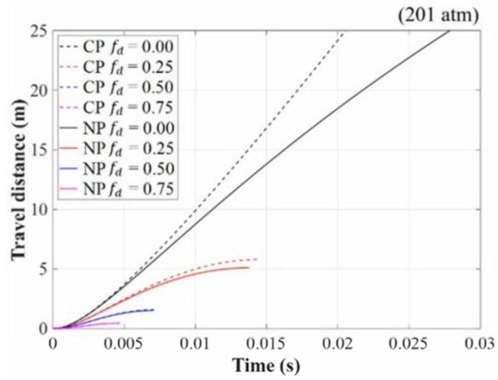

(a) Isothermal process

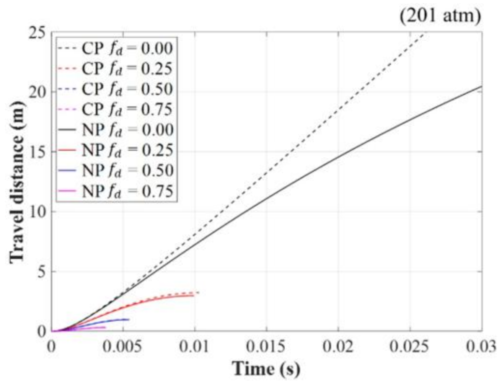

(b) Isentropic process

Fig. 11. Travel distance of the projectile over time in the isothermal and isentropic processes. CP is the constant tube pressure type, NP is the nonconstant tube pressure type, and f_d is the dimensionless friction.

1 % and 2 %, respectively.

In addition, in Fig. 11(b), the projectile of the NP travels up to 0.31 m with the dimensionless friction of 0.75. CP with the same dimensionless friction shows that the travels distance and travel time of the projectile are almost the same as those of NP with a difference of 0.5 % and 1.5 %, respectively. Therefore, because the compression wave magnitude is significantly smaller than the compressed air pressure behind the projectile, it represents that the effect of the compression wave is considerably smaller than the friction force as the dimensionless friction increases.

As shown in Fig. 11(a), in the case of NP, the projectile travels up to 5.1 and 1.5 m with the dimensionless friction of 0.25 and 0.5, respectively, but in the case of CP, projectile travels up to 5.8 and 1.6 m, respectively. As shown in Fig. 11(b), in the case of NP, the projectile travels up to 3 and 0.96 m with the dimensionless friction of 0.25 and 0.5, respectively, whereas for CP, the projectile travels up to 3.2 and 1 m, respectively.

Therefore, Fig. 11 shows that the travel distance of the projectile decreases owing to the effect of the compression wave as the friction force decreases. In addition, the travel distance and travel time of the projectile are greater in the isothermal process than in the isentropic process. In the isothermal process with the dimensionless friction of 0.5, the maximum velocity of the projectile appears at 0.6 m, and in the isentropic process with the same dimensionless friction, the maximum velocity of the projectile appears at 0.394 m.

Thus, it can be seen that for the same dimensionless friction, the isentropic process has a lower maximum velocity of the projectile than the isothermal process, and quickly reaches maximum velocity and then decreases.

3.2.2 Effect of change in the cross-sectional area and mass of the projectile

In this section, the velocity and travel distance of the projectile are analyzed by increasing the cross-sectional area and mass of the projectile, respectively, in the nonconstant tube pressure model. Table 2 lists the specifications for the cross-sectional area and mass of the projectile used in the analysis. To observe only the effect on the cross-sectional area or mass, a median value of 0.5 was selected from 0 to 1 for the dimensionless friction, and the expansion process of compressed air was investigated only in the isentropic process. The initial volume of the compressed air and the initial pressure of the compressed air are the same as in Sec. 3.2.1.

As shown in Figs. 12(a) and (b), the velocity of the projectile

Table 2. Comparison of the characteristics of the main parameters required for the analysis of the effect on the mass and cross-sectional area of the projectile. For example, ID A1-M1 denotes the case with the cross-sectional area of 0.7×10^{-5} m^2 and mass of 1.0×10^{-3} kg of the projectile.

Cross-sectional area of the projectile (m^2)	Mass of the projectile (kg)	ID
0.7×10^{-5}	1.0×10^{-3}	A1-M1
1.6×10^{-5}	1.0×10^{-3}	A2-M1
2.5×10^{-5}	1.0×10^{-3}	A3-M1
2.5×10^{-5}	1.5×10^{-3}	A1-M2
2.5×10^{-5}	2.0×10^{-3}	A1-M3
3.4×10^{-5}	1.0×10^{-3}	A4-M1

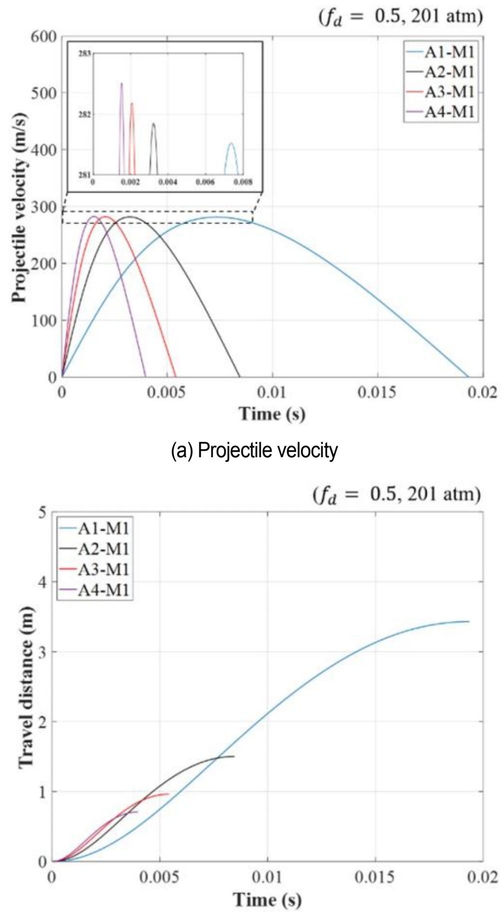

(a) Projectile velocity

(b) Travel distance

Fig. 12. Comparison of (a) velocity; (b) travel distance of the projectile according to time for an increase in the cross-sectional area of the projectile on the nonconstant tube pressure type. The dimensionless friction is 0.5, initial pressure of the compressed air is 201 atm, and the expansion process of the compressed air is isentropic process. The specifications of the projectile used are according to the ID in Table 2.

increases as the cross-sectional area of the projectile increases. Conversely, as the cross-sectional area of the projectile increases, the travel time and travel distance of the projectile decreases. However, a comparison of the maximum velocities of the projectiles of A1-M1 and A4-M1 indicates that they are almost the same with a difference of around 1 m/s. Conversely, the travel distance of the projectile between A1-M1 and A4-M1 is 2.72 m, implying a large difference.

As the cross-sectional area of the projectile increases, the force with which the compressed air behind the projectile pushes against the projectile increases. Simultaneously, as the cross-sectional area of the projectile increases, the force that disturbs the movement of the projectile by the pressure of the tube in front of the projectile increases. However, as the tube pressure in front of the projectile is very small compared to the pressure of compressed air, the effect of the tube pressure in front of the projectile on the increase of the total force acting on the projectile is very small.

In addition, the dimensionless friction is fixed at 0.5, but the friction force increases as the cross-sectional area of the projectile increases, because it is expressed as the product of the cross-sectional area of the projectile and the initial pressure of the compressed air. However, as the cross-sectional area increases, the total force acting on the projectile is most affected by the force applied by the compressed air behind the projectile pushing the projectile. The pressure change of the compressed air behind the projectile with time has only one variable, the travel distance $x(t)$ of the projectile, as shown in Eq. (7). Therefore, as the cross-sectional area increases, the force owing to the pressure of the compressed air rapidly increases, so the travel distance of the projectile decreases rapidly.

Conversely, the change in the maximum magnitude of the compression wave in front of the projectile is very small because the effect of the air in the tube on the total force acting on the projectile is small when the cross-sectional area increases.

Therefore, the change in the maximum velocity of the projectile, which is directly related to the compression wave magnitude, is very small compared to the change in the maximum travel distance of the projectile.

Fig. 13 shows the total force acting on the projectile with an increase in the cross-sectional area of the projectile, magnitude of the compression wave generated in the tube in front of the projectile, force of the compressed air behind the projectile to push the projectile, and compressed air pressure according to the travel time of the projetile.

In Fig. 13(c), the driving force refers to the force that pushes the projectile with the expansion of the compressed air in the reservoir behind the projectile. Fig. 13(a) shows that when the cross-sectional area of the projectile increases from A1 to A4,

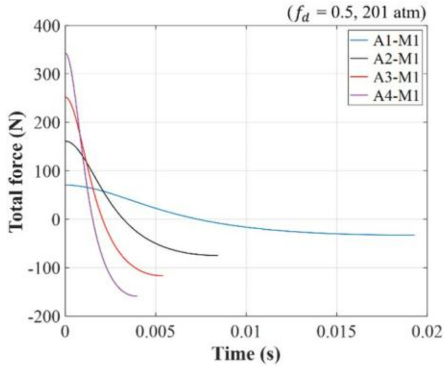

(a) Total force

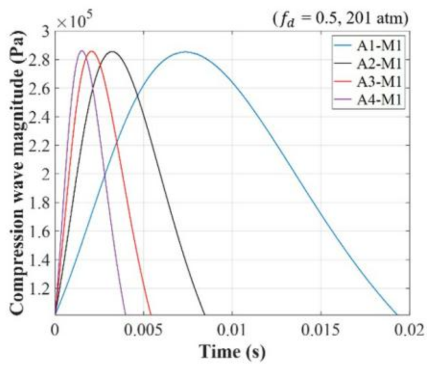

(b) Compression wave magnitude

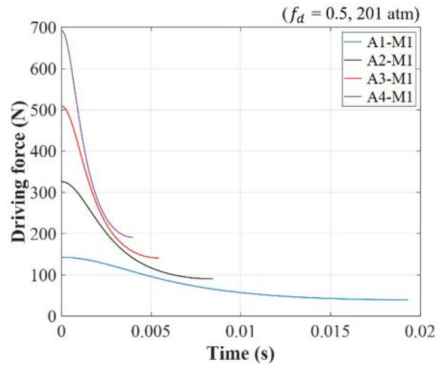

(c) Driving force

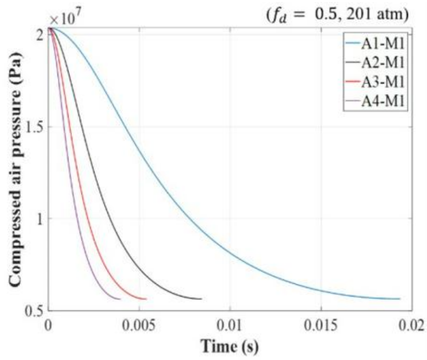

(d) Compressed air pressure

Fig. 13. Comparison of (a) total force; (b) compression wave magnitude; (c) driving force; (d) compressed air pressure for an increase in the cross-sectional area of the projectile on the constant tube pressure type. The dimensionless friction is 0.5, initial pressure of the compressed air is 201 atm, and the expansion process of the compressed air is isentropic process. The specifications of the projectile used are according to the ID in Table 2.

the total force acting on the projectile at t = 0 s increases by five times and then decreases sharply thereafter.

As described in Fig. 12, this is most affected by the driving force, which is the force that the expanding compressed air behind the projectile pushes the projectile. Therefore, the driving force increases as the cross-sectional area of the projectile increases, and the total force acting on the projectile increases.

In addition, Fig. 13(b) shows that the magnitude of the compression wave increases as the cross-sectional area of the projectile increases, but the maximum value difference between the A1-M1 and A4-M1 is relatively small at 0.3 %. The change in the magnitude of the compression wave in front of the projectile in Fig. 13(b) is a significantly smaller than the change in the compressed air pressure behind the projectile in Fig. 13(d).

Therefore, because the velocity of the projectile is eventually determined by the compression wave Mach number, the change in the maximum velocity of the projectile is small, equal to the magnitude of the compression wave. The variable of the driving force has only the travel distance $x(t)$ by Eq. (7).

Therefore, the maximum travel distance of the projectile decreases as the maximum value of the driving force increases.

Figs. 14(a) and (b) show the effect of increasing the mass of the projectile on the velocity and distance of the projectile. As the mass of the projectile increases, the maximum velocity of the projectile decreases and the maximum travel distance of the projectile increases. In addition, the travel time of the projectile increases.

In Fig. 14(a), comparing the maximum velocity of the projectile of the A3-M1 and A3-M3, the maximum velocity of the projectiles is 282 and 200 m/s, showing a difference of approximately 82 m/s. However, in Fig. 14(b), comparing the maximum travel distance of the projectiles of A3-M1 and A3-M3, the maximum travel distances are 0.96 and 0.97 m, respectively, which are almost the same. Therefore, the maximum velocity of the projectile shows a significant difference as the mass of the projectile increases, while the maximum travel distance of the projectile shows almost similar results.

As the mass of the projectile increases, the initial acceleration of the decreases. In Eq. (8), the change in the mass of the projectile does not directly affect the force owing to the pressure in front and behind of the projectile and the friction force.

As the mass of the projectile increases, the initial total force remains the same and the initial acceleration of the projectile decreases. Therefore, as the initial acceleration of the projectile decreases, the maximum velocity of the projectile decreases and the maximum velocity appears late.

As the mass of the projectile increases, the initial total force acting on the projectile remains the same, so the velocity of the projectile decreases and travel time increases, the maximum

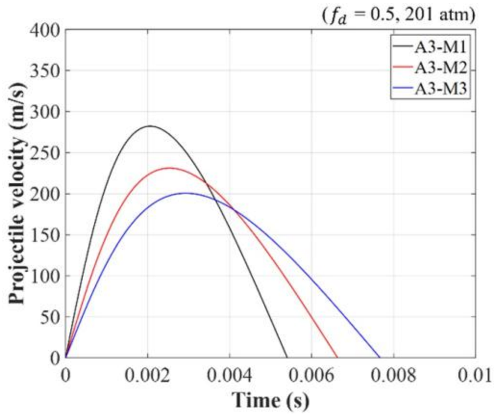

(a) Projectile velocity

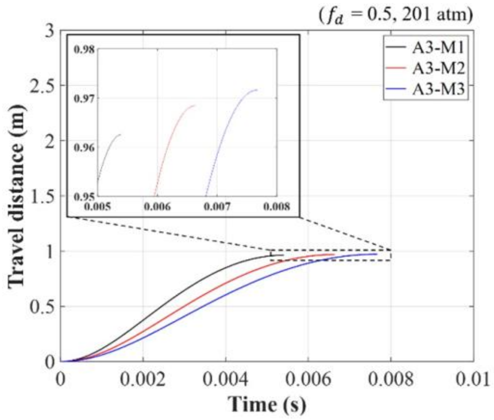

(b) Travel distance

Fig. 14. Comparison of (a) velocity; (b) travel distance of the projectile according to time for an increase in the mass of the projectile on the non-constant tube pressure type. The dimensionless friction is 0.5, initial pressure of the compressed air is 201 atm, and the expansion process of the compressed air is isentropic process. The specifications of the projectile used are according to the ID in Table 2.

travel distance does not change significantly.

Fig. 15 shows the total force acting on the projectile with an increase in the mass of the projectile, pressure of the compressed air behind the projectile, force by the tube pressure in front of the projectile, and acceleration of the projectile according to the travel time of the projectile. In Fig. 15(c), the resistance force represents the force due to the pressure of the air in the tube in front of the projectile, which disturbs the movement of the projectile.

As the mass of the projectile increases, the total force acting on the projectile will have the same force at t = 0 s with a different tendency than the cross-sectional area of the projectile, as shown in Fig. 15(a). Thereafter, as the mass increases, the total force decrease slowly, thereby decreasing the velocity of the projectile and increasing the travel time. The total force acting on the projectile is most affected by the force of the compressed air behind the projectile. However, the pressure of the compressed air behind the projectile is not affected by the mass of the projectile according to Eq. (7).

Therefore, as shown in Fig. 15(b), although the mass of the projectile increases, the compressed air pressure changes in the same trend as the total force acting on the projectile. Conversely, as shown in Fig. 15(c), the magnitude of the compression wave generated in the tube in front of the projectile decreases repidly as the mass increases, so the resistance force, which is the force by the tube pressure in front of the projectile, also rapidly decreases.

In Fig. 15(d), as the mass of the projectile increases, the initial acceleration of the projectile decreases and the travel time of the projecitle increases. In other words, as the mass of the projectile increases, the initial acceleration of the projectile decreases because the initial value of the total force acting on the projectile remains the same. As the acceleration of the projectile decreases, the velocity of the projectile and magnitude of the compression wave sharply decreases, and the travel time of the projectile increases, so the change in the travel distance of t he projectile is relatively small.

3.2.3 The effect of the compressed air initial pressure in the reservoir

For the nonconstant tube pressure, the initial pressure of the compressed air in the reservoir was gradually increased and analyzed. The initial pressure of the compressed air was increased for analysis, and the volume of the reservoir remained constant at V_0 = 1.6×10^{-3} m^3. The cross-sectional area of the projectile was A_1 = 2.5×10^{-5} m^2, and the mass of the projectile was m_1 = 1.0×10^{-3} kg.

The initial pressure of the compressed air was sequentially increased to 11, 51, 101, and 201 atm, and as in the Sec. 3.2.1, the dimensionless friction increased by 0.25 in the range of 0-0.75 except for 1, where the projectile was stationary. For the expansion process of the compressed air, only the isentropic process was analyzed, and the ID in Table 1 was applied according to the initial pressure of the compressed air.

Fig. 16 shows the velocity of the projectile according to the travel time and dimensionless friction with a gradual increase in the initial pressure of the compressed air. The velocity of the projectile increases as the initial pressure of the compressed air increases. In other words, as the initial pressure of the compressed air increases, the maximum velocity of the projectile increases, the travel time decreases, and the maximum velocity appears faster. In addition, as the dimensionless friction increases, the velocity, travel distance, and travel time of the projectile decrease.

In Fig. 16, when the dimensionless friction was 0.5, the maximum velocity of the projectile was 50.8 m/s for NP011, 135 m/s for NP051, 196.6 m/s for NP101, and 282.2 m/s for NP201. In Fig. 16, for an increase of 100 atm (around 99 %) from NP101 to NP201, the maximum velocity of the projectile increased by 85.6 m/s (approximately 43 %). However, a comparison of A1-M1 and A2-M1 in Fig. 12(a) of Sec. 3.2.2 reveals that the maximum velocity of the projectile increased by 0.11 % compared to the 130 % increase in the cross-sectional area of the projectile. In addition, comparing A3-M1 and A3-M3 in Fig.

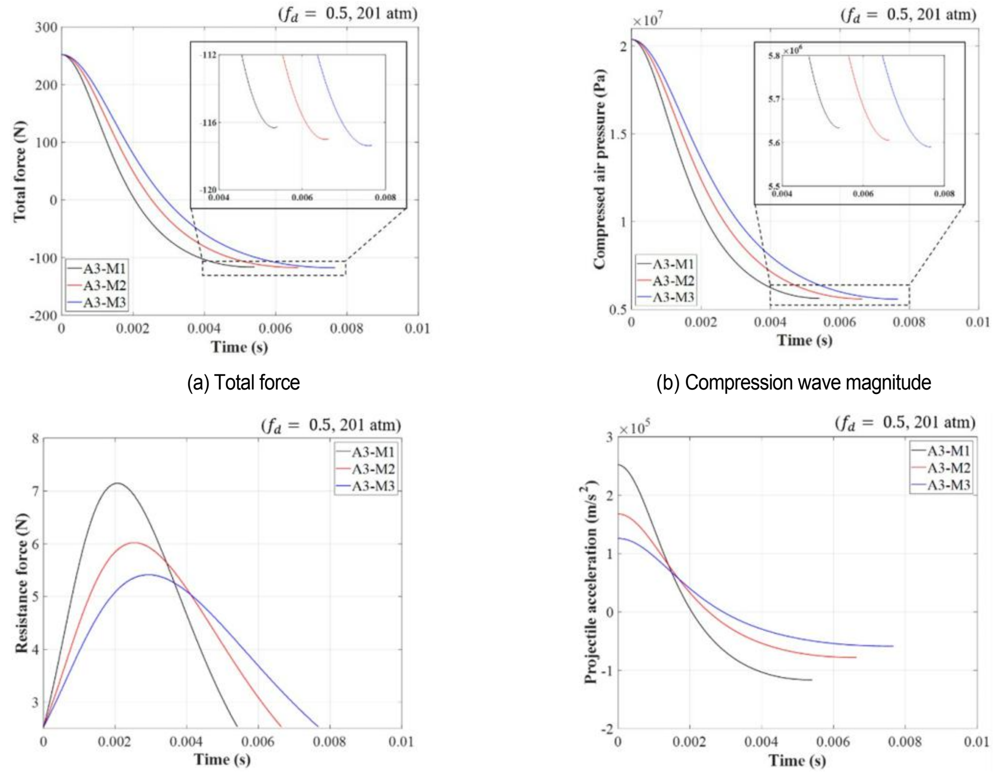

(a) Total force
(b) Compression wave magnitude
(c) Driving force
(d) Compressed air pressure

Fig. 15. Comparison of (a) total force; (b) compressed air pressure; (c) resistance force; (d) projectile acceleration according to time for an increase in the mass of the projectile on the nonconstant tube pressure type. The dimensionless friction is 0.5, initial pressure of the compressed air is 201 atm, and the expansion process of the compressed air is isentropic process. The specifications of the projectile used are according to the ID in Table 2.

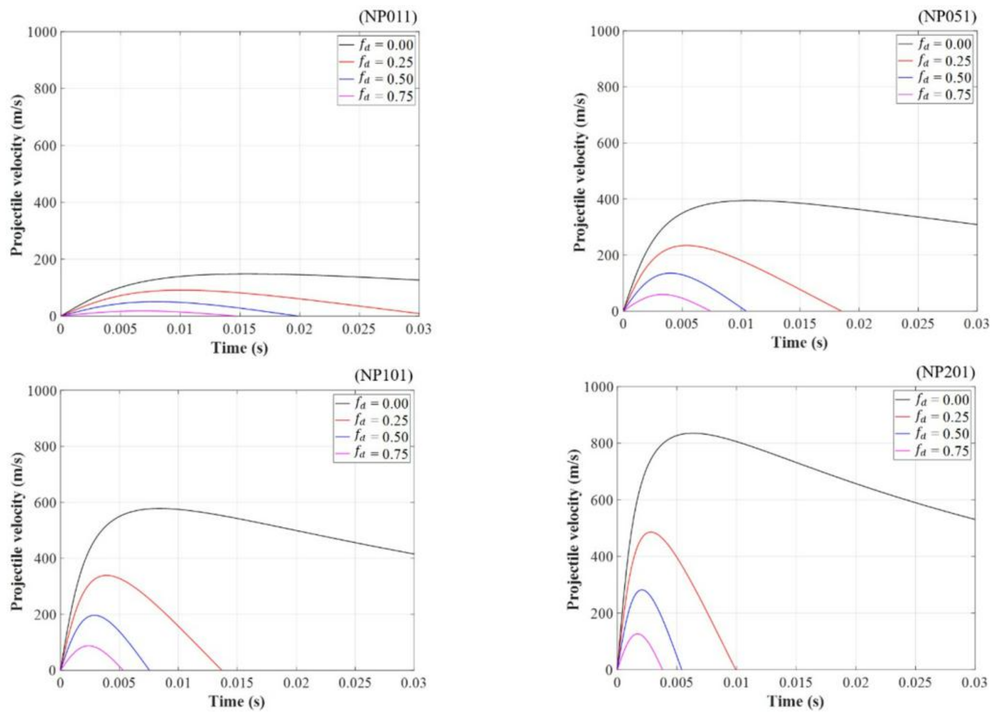

Fig. 16. Velocity of the projectile versus time for the initial pressure increase of the compressed air in the reservoir. The expansion process of the compressed air is the isentropic process, f_d is the dimensionless friction, and the ID given in Table 1 is followed according to the initial pressure of the compressed air (11, 51, 101, and 201 atm).

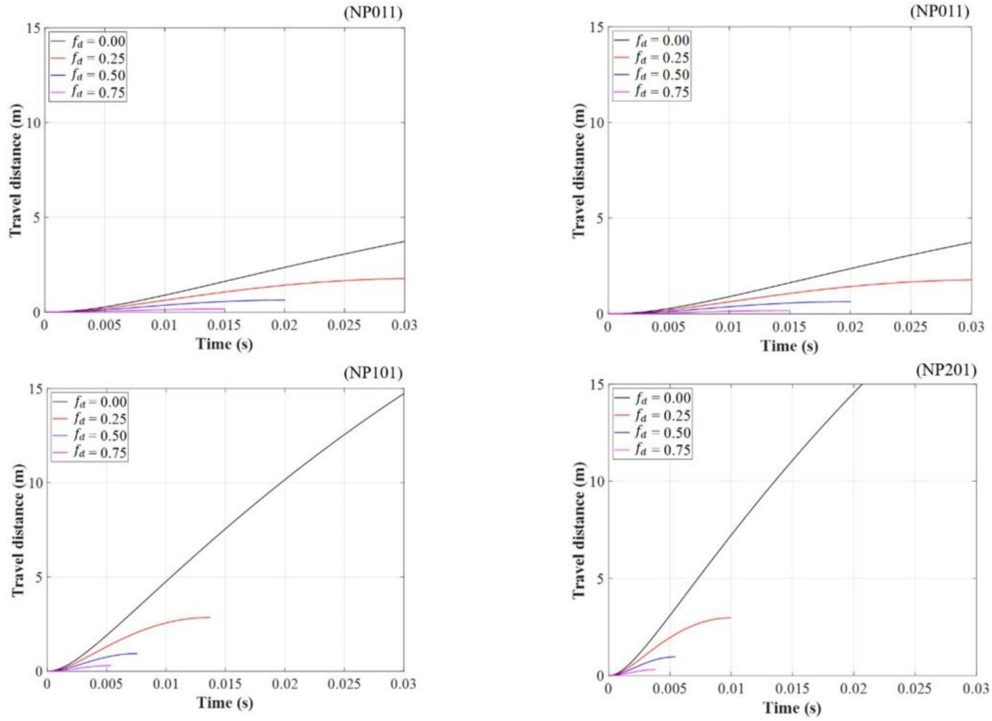

Fig. 17. Travel distance of the projectile versus time for the initial pressure increase of the compressed air in the reservoir. The expansion of the compressed air is the isentropic process, f_d is the dimensionless friction, and the ID given in Table 1 is followed according to the initial pressure of the compressed air.

14(a) in Sec. 3.2.2 reveals that the maximum velocity of the projectile decreases by around 41 % from 282 to 200 m/s as the mass of the projectile increases by 100 %.

Therefore, the change in the initial pressure of the compressed air behind the projectile had the greatest effect on the change in the maximum velocity of the projectile than the change in the cross-sectional area and mass of the projectile [25].

As the initial pressure of the compressed air increases, the travel distance of the projectile increases and the travel time decreases. Further, as dimensionless friction increases, the travel distance and travel time decrease. In Fig. 17, when the dimensionless friction was 0.5, the maximum travel distance of the projectile was approximately 0.637, 0.889, 0.935, and 0.963 m for NP011, NP051, NP101, and NP201, respectively. Therefore, as the initial pressure of the compressed air increases, the maximum travel distance increases.

In Fig. 17, when the initial pressure of the compressed air increased by around 100 % from 101 to 201 atm, the maximum travel distance of the projectile increased by approximately 3 % from 0.935 to 0.963 m. Comparing A3-M1 and A3-M3 in Fig. 14(b) in Sec. 3.2.2 reveals that the maximum travel distance of the projectile increases by around 1 % from 0.96 to 0.97 m as the mass of the projectile increases by 100 %. However, comparing A1-M1 and A2-M1 in Fig. 12(b) in Sec. 3.2.2 indicates that the maximum travel distance of the projectile decreases by approximately 130 % from 3.43 to 1.5 m as the cross-sectional area of the projectile increases by around 130 %.

Therefore, the change in the initial pressure of the compressed air of the projectile affects the maximum travel distance of the projectile more than the change in the mass of the projectile, but the change in the cross-sectional area of the projectile has the greatest effect.

4. Conclusions

The behavior of the projectile was predicted by developing a theory assuming the tube pressure in front of the projectile as a variable considering the effect of the compression wave generated in front of the projectile moving in the tube of the compressed air cannon. As a result, the maximum velocity of the projectile of the nonconstant tube pressure type was lower than the constant tube pressure type in the entire range of the dimensionless friction.

The maximum velocity difference between the constant and nonconstant tube pressures type increases as the dimensionless friction decreases. In other words, the maximum velocity of the projectile reduced owing to the compression wave in the nonconstant tube pressure type. Furthermore, the compression wave decreased not only the maximum velocity of the projectile, but also the maximum velocity occurrence point, acceleration, and maximum travel distance of the projectile. The maximum velocity of the projectile in the constant tube pressure type occurs near the maximum travel distance of the projectile. However, when the compression wave is considered, the maximum velocity of the projectile occurs much faster, and then the velocity gradually decreases.

As the cross-sectional area of the projectile increases, the maximum travel distance of the projectile decreases sharply, while the maximum velocity increases slightly. Thus, the change in the cross-sectional area of the projectile affects the force by the compressed air behind the projectile, so the travel distance of the projectile changes rapidly. As the mass of the projectile increases, the maximum velocity of the projectile decreases sharply, while the maximum travel distance increases slightly. Therefore, the change in the mass of the projectile affects the force by the tube pressure in front of the projectile, so the velocity of the projectile changes rapidly.

The change in the initial pressure of the compressed air behind the projectile has a greatest effect on the change in the maximum velocity of the projectile than the change in the cross-sectional area and mass of the projectile. In addition, the change in the initial pressure of the compressed air affects the travel distance of the projectile more than the change in the mass of the projectile, but the change in the cross-sectional area of the projectile has the greatest effect on the change in the travel distance.

The present study has several limitations. The assumption of the isothermal expansion cannot be applied when the projectile is traveling at the speed of sound, the velocity of the projectile in the isothermal process can be more dissimilar to the actual operation than in the isentropic process [3]. Conversely, the theoretical development in the isentropic process is not limited by the speed of sound. In fact, it can be applied similarly to the adiabatic process by using a non-metallic material that does not transfer heat.

This study assumed that the projectile and the tube had the same cross-sectional area, so there was no compressed air leakage through the gap. However, the compression wave is affected by the leakage of compressed air. In particular, the air leakage changes the flow quantities between the projectile and compression wave. Further, because the length of the projectile was not used, the friction force was expressed as the initial pressure of the compressed air behind the projectile and the cross-sectional area of the projectile, and the friction force was assumed to be constant. Thus, while we can anticipate the predictions for constant friction to be approximate, the simplifications of our model means that we can derive an analytical expression for the behavior of the projectile [3]. Next, as a result of using our theoretical model, it can be seen that the traveling distance of the projectile exceeds 20 m when the dimensionless friction is zero. Because the tube length has a significant effect on the behavior of the projectile, the actual behavior in long tubes may differ from our findings. However, It is plotted only to see the effect of the compression wave acting on the projectile under the assumption that there is no friction force. Although it is not realistic to include the results of dimensionless friction 0 with no frictional force and dimensionless friction 1 with maximum frictional force, it is intended to analyze the effect of compression waves on projectiles in drastic cases.

Therefore, in future study, we plan to analyze efficient and realistic parameters such as appropriate tube length, projectile mass, and cross-sectional area through our theoretical model. In addition, we plan to consider verification of the isothermal and adiabatic processes through simulation, definition of change in the friction force, and the compressed air leakage through the blockage ratio.

Acknowledgments

This research was supported by the Ministry of Trade, Industry & Energy (MOTIE) of the Republic of Korea under the Fostering Global Talents for Innovative Growth Program [No. P0017308] supervised by the Korea Institute for Advancement of Technology (KIAT), by the “Core Technology Development of Subsonic Capsule Train” of the Korea Railroad Research Institute [No. PK2301A1], and by the Chung-Ang University Research Scholarship Grants in 2021.

Nomenclature

a : Acceleration of projectile (m/s^2)
A : Cross-sectional area of projectile (m^2)
f : Friction force (N)
f_d : Dimensionless friction
F : Total force acting on projectile (N)
L : Length of tube (m)
m : Mass of projectile (kg)
M : Mach number
P_{atm} : Atmosphere pressure ($kg/(m \cdot s^2)$)
P : Pressure of compressed air behind projectile ($kg/(m \cdot s^2)$)
γ : Specific heat ratio
R : Individual gas constant
t : Travel time of projectile
T : Tube air temperature (K)
v : Velocity of projectile (m/s)
V : Volume of compressed air behind projectile (m^3)
x : Travel distance of projectile (m)

Superscript

s : Shock-relative coordinate system

Subscript

0 : Initial state of compressed air cannon
1 : Local quantity behind shock wave
2 : Local quantity in front of shock wave
s : Shock wave

References

[1] Z. J. Rohrbach, T. R. Buresh and M. J. Madsen, Modeling the exit velocity of a compressed air cannon, *American Journal of Physics*, 80 (1) (2012) 24-26.
[2] C. E. Mungan, Internal ballistics of a pneumatic potato cannon, *European Journal of Physics*, 30 (3) (2009) 453.
[3] M. Denny, The internal ballistics of an air gun, *The Physics*

Teacher, 49 (2) (2011) 81-83.
[4] E. Ayars and L. Buchholtz, Analysis of the vacuum cannon, *American Journal of Physics*, 72 (7) (2004) 961-963.
[5] G. Olson, R. Peterson, B. Pulford, M. Seaberg, K. Stein, C. Stelter and R. Weber, The role of shock waves in expansion tube accelerators, *American Journal of Physics*, 74 (12) (2006) 1071-1076.
[6] R. W. Peterson, B. N. Pulford and K. R. Stein, The ping-pong cannon: A closer look, *The Physics Teacher*, 43 (1) (2005) 22-25.
[7] R. M. French, V. Gorrepati, E. Alcorta and M. Jackson, The mechanics of a ping-pong ball gun, *Experimental Techniques*, 32 (1) (2008) 24-30.
[8] Z. Jiang, Wave dynamic processes induced by a supersonic projectile discharging from a shock tube, *Physics of Fluid*, 15 (6) (2003) 1665-1675.
[9] Z. L. Jiang, K. Takayama and B. W. Skews, Numerical study on blast flowfields induced by supersonic projectiles discharged from shock tubes, *Physics of Fluid*, 10 (1) (1998) 277-288.
[10] R. Gopalapillai, H. D. Kim, T. Setoguchi and S. Matsuo, On the near-field aerodynamics of a projectile launched from a ballistic range, *Journal of Mechanical Science and Technology*, 21 (2007) 1129-1138.
[11] G. Zhang, D. H. Kim and H. D. Kim, Numerical analysis of impulse waves discharged at the exit of a model tunnel, *Journal of Mechanical Science and Technology,* 32 (2018) 2099-2109.
[12] C. M. Athira, G. Rajesh, S. Mohanan and A. Parthasarathy, Flow interactions on supersonic projectiles in transitional ballistic regimes, *Journal of Fluid Mechanics*, 894 (2020) A27.
[13] B. Auvity and M. Bellenoue, Effects of an opening on pressure wave propagation in a tube, *Journal of Fluid Mechanics*, 538 (2005) 269-289.
[14] T. G. Keith and J. E. John, *Gas Dynamics*, Pearson, England (2006).
[15] K. S. Jang, T. T. G. Le, J. Kim, K. S. Lee and J. Ryu, Effect of compressible flow phenomena on aerodynamic characteristics in Hyperloop system, *Aerospace Science and Technology*, 117 (2021) 106970.
[16] J. Ma, Z. Chen, D. Xue and X. Sun, Influences of boattail structures on aerodynamic characteristics of supersonic spinning projectiles, *Theoretical and Computational Fluid Dynamics*, 34 (2020) 249-270.
[17] M. Denny, Gas gun dynamics, *European Journal of Physics*, 34 (5) (2013) 1327.
[18] D. H. Kim and I. G. Oh, Development of 1/60th scale moving model rig using the compressed air launcher and one-wire guidance system of train model, *Transactions of the Korean Society of Mechanical Engineers B*, 25 (2001) 634-644.
[19] A. Ferrari, Analytical solutions for one-dimensional diabatic flows with wall friction, *Journal of Fluid Mechanics*, 918 (2021) A32.
[20] S. R. Yeddula, J. Guzmán-Iñigo and A. S. Morgans, A solution for the quasi-one-dimensional linearized Euler equations with heat transfer, *Journal of Fluid Mechanics*, 936 (2022) R3.
[21] M. Singh and A. Patel, Shock wave structure in a non-ideal gas under temperature and density-dependent viscosity and heat conduction, *Theoretical and Computational Fluid Dynamics*, 33 (6) (2019) 537-559.
[22] A. Sasoh, S. Ohba and K. Takayama, Quantitative effects of projectile-launch tube wall friction on ballistic range operation, *AIAA Journal*, 38 (9) (2000) 1709-1715.
[23] Q. Yu, X. Yang, J. Niu, Y. Sui, Y. Du and Y. Yuan, Theoretical and numerical study of choking mechanism of fluid flow in Hyperloop system, *Aerospace Science and Technology*, 121 (2022) 107367.
[24] K. Oswatitsch, Intermediate ballistics, W. Schneider and M. Platzer (eds), *Contributions to the Development of Gasdynamics*, Vieweg+Teubner Verlag (1980) https://doi.org/10.1007/978-3-322-91082-0_21.
[25] D. H. Kim and B. B. Kang, Experimental study about the effect of a partial vacuum in the tunnel on the speed-up of a super-speed train model of moving model test rig, *The Ninth World Congress on Railway Research,* Lille, France (2011) 1-8.

Woojin Sung is the master's course of the School of Mechanical Engineering, Chung-Ang University, Seoul, Korea. He received his B.S. in Mechanical Engineering from Chung-Ang University. His research topic is analysis of compressible flow phenomenon such as shock tube and Hyperloop system.

Jihoon Kim is currently pursuing his Ph.D. in Mechanical Engineering. He received his B.S. in Mechanical Engineering from Chung-Ang University, Seoul, Korea. His research interests include shock waves and aerodynamics for compressible flow, pool and flow boiling simulation.

Thi Thanh Giang Le started studying for Master's degree in Mechanical Engineering at Chung-Ang University. She received a B.S. as Engineering Mechanics in the Faculty of Applied Sciences at Ho Chi Minh University of Technology, Viet Nam. Her research topic is numerical analysis of aerodynamic characteristics of Hyperloop System.

Kyeong Sik Jang is received his M.S. in Mechanical Engineering at Chung-Ang University in 2022. His research topic is study of stenosis induced flow in blood vessels with acoustic analysis methods. He also studies about bruit detection occurring in carotid stenosis and Hyperloop system.

Jeonglae Kim is a Professor in the School for Engineering of Matter, Transport and Energy, at Arizona State University, USA. He obtained his Ph.D. in Theoretical and Applied Mechanics at University of Illinois-Urbana-Champaign. His research interests include large-eddy simulation of high-speed turbulent flows with multi-physics, aeroacoustics, flow control and optimization.

Dong Hyeon Kim received his B.S. and M.S. degrees from Chung-Ang University, Korea in 1986 and 1988. He then received his Ph.D. from Seoul National University, Korea in 1993. Currently, Dr. Kim is an Executive Researcher in Korea Railroad Research Institute (KRRI). His research interests include high-speed trains, subsonic speed capsule train, tunnel aerodynamics, micro-pressure wave, moving model test rig.

Hyoungsoon Lee is a Professor in the School of Mechanical Engineering at Chung-Ang University, Seoul, Korea. He obtained his Ph.D. at Purdue University. His research interests include heat transfer, electronic packaging, microfluidic heat sink, energy conversion devices for flexible electronics, data centers, and high power electronic systems.

Jaiyoung Ryu is a Professor in the School of Mechanical Engineering at Korea University, Seoul, Korea. He obtained his Ph.D. in Mechanical Engineering at Stanford University, USA. His research interests include compressible turbulence, Hyperloop, computational fluid dynamics, gas turbine, and cardiovascular hemodynamics.